Mechanistic and Kinetic Study of the O + CH_2OH Reaction

Hua Hou and Baoshan Wang*

College of Chemistry and Molecular Sciences, Wuhan University, Wuhan 430072, People's Republic of China

Received: March 8, 2005; In Final Form: April 15, 2005

The mechanism for the O + CH_2OH reaction was investigated by various ab initio quantum chemistry methods. For the chemical activation mechanism, that is, the addition/elimination path, the couple-cluster methods including CCSD and CCSD(T) were employed with the cc-pV*X*Z (*X* = D, T, Q, 5) basis sets. For the abstraction channels, multireference methods including CASSCF, CASPT2, and MRCISD were used with the cc-pVDZ and cc-pVTZ basis sets. It has been shown that the production of H + HCOOH is the major channel in the chemical activation mechanism. The minor channels include HCO + H_2O and OH + CH_2O. The hydrogen abstraction by an O atom from the CH_2OH radical produces either OH + CH_2O or OH + HCOH. Moreover, the two abstraction reactions are essentially barrierless processes. The rate constants for the association of O with CH_2OH have been calculated using the flexible transition state theory. A weak negative temperature dependence of the rate constants is found in the range 250−1000 K. Furthermore, it is estimated that the abstraction processes also play an important role in the O + CH_2OH reaction. Additionally, the falloff behavior for the $OCH_2OH \rightarrow$ H + HCOOH reaction has been investigated. The present theoretical results are compared to the experimental measurements to understand the mechanism and kinetic behavior of the O + CH_2OH reaction and the unimolecular reaction of the OCH_2OH radical.

I. Introduction

The gas-phase reactions between two radicals have attracted considerable attention because they play important roles in combustion, flame, and atmosphere. Such reactions are always very fast and always involve numerous product channels. Therefore, the understanding of the radical−radical reaction is a challenge to both experimentalists and theorists.

As alcohols have become more widely used as alternative fuels and fuel additives, there is an increasing need to understand the chemistry of their combustion processes. The $O(^3P)$ + CH_2OH reaction is a key process in the oxidation of methanol. It has been found that the reaction proceeds very fast with a near gas-collision rate. Grotheer et al. measured the room-temperature rate constant for the O + CH_2OH reaction using mass spectroscopy.[1] A value of 1.5×10^{-10} cm^3 $molecule^{-1}$ s^{-1} was determined by simulating a complex multistep mechanism. Seetula et al. performed a direct measurement on the O + CH_2OH reaction using a heatable tubular reactor and a photoionization mass spectrometer.[2] Over the temperature range 300−508 K, the rate constants are independent of pressures and show negative temperature dependence. Both formaldehyde and formic acid were detected as products of the O + CH_2OH reaction. However, their yields are still unknown.

An ab initio quantum chemistry computational study is very useful for characterizing the reaction mechanism. Moreover, the rate constants for the multiple product channels could be predicted, and thus, the dominant nascent products could be known as well. There is no theoretical study reported on the O + CH_2OH reaction up to date.

In this paper, high-level ab initio calculations were carried out for the title reaction. Besides the well-known "chemical activation" mechanism (i.e., addition/elimination), the direct abstraction channel was shown to be of equal importance in the O + CH_2OH reaction. The overall rate constants were also calculated using the flexible transition state theory and compared to the experimental data. Moreover, the kinetics for the $OCH_2OH \rightarrow$ H + HCOOH reaction was also studied to understand the mechanism of the formic acid formation.

II. Computational Methods

Only the doublet potential energy surface in the lowest electronic state has been investigated. The geometries of various species including the intermediates and the transition states were first optimized using the couple-cluster theory with the single and double excitations, namely, CCSD,[3] with the cc-pVDZ basis set.[4] All species were subject to harmonic frequency analysis at the same level to calculate the zero-point energies and to determine the nature of the stationary points. A transition state has only one imaginary frequency. The intrinsic reaction coordinate (IRC)[5] calculation confirms that the transition state connects the desired reactants and products.

The geometrical parameters were refined using the larger cc-pVTZ basis set.[4] It is well-known that spin contamination is always a serious problem for the open-shell reaction system if the unrestricted single-determinant Hartree−Fock (HF) reference wave function is used. Therefore, the restricted open-shell couple-cluster theory[6] with single, double, and noniterative triple excitation [RCCSD(T)] based on the restricted open-shell Hartree−Fock (ROHF) reference, with Dunning's cc-pVTZ and cc-pVQZ basis sets,[4] was employed to calculate the total energies of all species at the CCSD/cc-pVTZ optimized geometries.

Two schemes were employed to estimate the full configuration interaction (CI) limit for comparison. The first scheme is an empirically motivated approach based on the use of a

* Corresponding author. E-mail: wangb@chem.whu.edu.cn. Fax: 86-27-6875-4067.

10.1021/jp051189+ CCC: $30.25 © 2005 American Chemical Society
Published on Web 05/11/2005

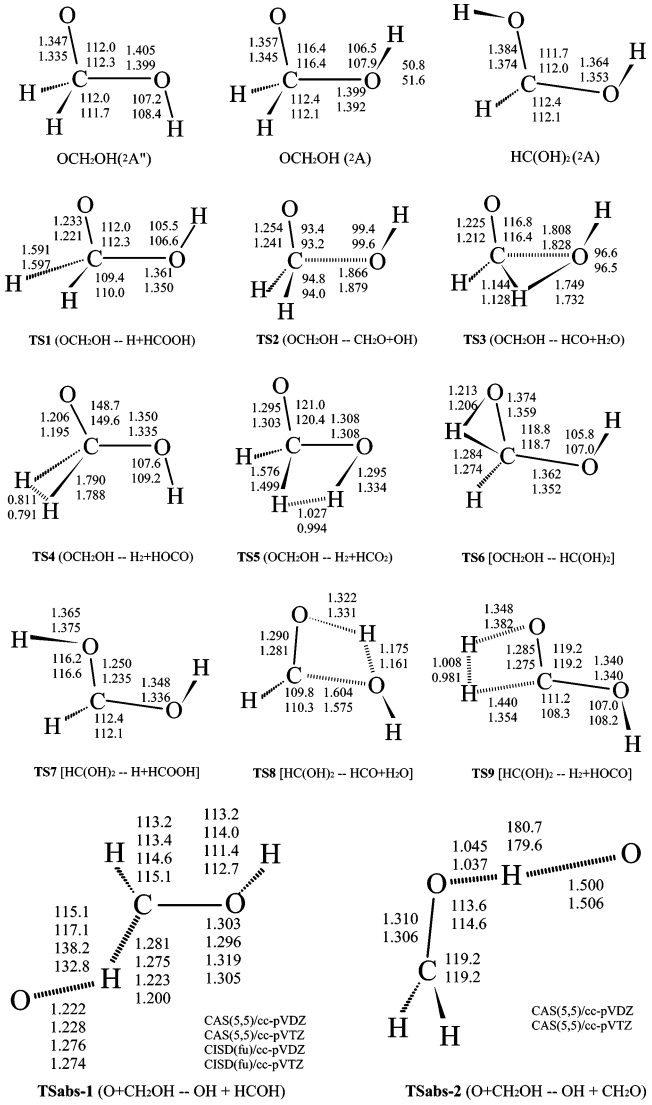

Figure 1. CCSD/cc-pVDZ (upper) and CCSD/cc-pVTZ (lower) optimized geometries for the intermediates and transition states involved in the O(^{3}P) + CH_2OH reaction. The bond distances are in angstroms, and the bond angles are in degrees. For **TSabs-1** and **TSabs-2**, the entries are indicated beside the graphics.

continued fraction (cf) approximant[7] with the RCCSD(T)/cc-pVQZ energies:

$$E_{\mathrm{cf}} = \frac{\delta_1}{1 - \dfrac{\delta_2/\delta_1}{1 - \delta_3/\delta_2}}$$

where $\delta_1 = E_{\mathrm{SCF}}$, $\delta_2 = E_{\mathrm{CCSD}} - E_{\mathrm{SCF}}$, and $\delta_3 = E_{\mathrm{CCSD(T)}} - E_{\mathrm{CCSD}}$. In the second scheme, the correlation energies obtained at the RCCSD(T)/cc-pVTZ and RCCSD(T)/cc-pVQZ levels were used to estimate the complete basis set (CBS) limit according to the formula $E_{\mathrm{corr}}^{\infty} = E_{\mathrm{corr}}^{X} + aX^{-3}$ ($X = 3$ and 4 for cc-pVTZ and cc-pVQZ, respectively).[8] The ROHF CBS limit was obtained by extrapolating three energies calculated using the cc-pVTZ, cc-pVQZ, and cc-pV5Z basis sets according to the formula $E_{\mathrm{HF}}^{\infty} = E_{\mathrm{HF}}^{X} + a\exp(-bX)$.[9] Note that the extrapolation parameters a, b, $E_{\mathrm{corr}}^{\infty}$, and E_{HF}^{∞} are uniquely determined from the corresponding energies.

While the couple-cluster theory can account for most of the electron correlation energies, we found that the nondynamical electron correlation effect is inherently significant in the transition states for the abstraction channels, as indicated by the expectation value of S^2 of the HF determinant. Therefore, the multireference self-consistent field (SCF) methods were employed to describe such reaction paths correctly. The geometries of the transition states for the two abstraction reactions, namely, O(^{3}P) + $CH_2OH \rightarrow OH + CH_2O$ and O(^{3}P) + $CH_2OH \rightarrow OH + HCOH$, were optimized using the complete active space (CAS) SCF[10] with the cc-pVDZ and cc-pVTZ basis sets. The active space includes five electrons in five orbitals. The barrier heights were calculated using both the multireference second-order Moller−Plesset theory (CASPT2)[11] and the multireference configuration interaction theory (MRCISD).[12]

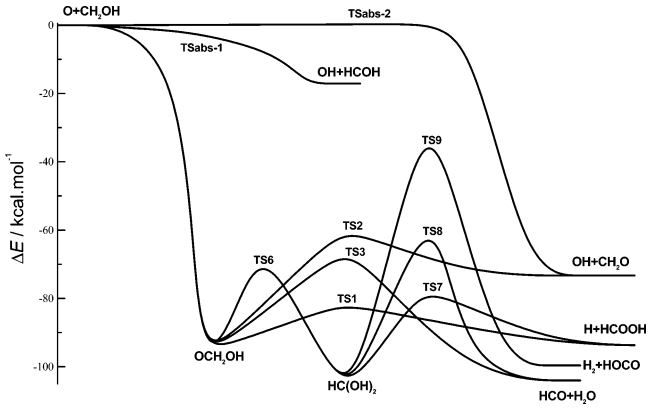

Figure 2. Profile of the potential energy surface for the O(^{3}P) + CH_2OH reaction. The indicated energies (ΔE, in kilocalories per mole) were calculated at the RCCSD(T)/CBS level with zero-point energy corrections. Note that **TS4** and **TS5** of no importance are excluded for clarity. The two abstraction paths are essentially barrierless.

All the geometry optimization and frequency calculations were performed using the Gaussian programs.[13] All the single-point energy calculations were carried out using the Molpro program.[14] The kinetic calculations were done with the Variflex program,[15] and the details will be listed separately.

III. Results and Discussion

Two types of mechanisms have been found for the O + CH_2OH reaction. The first mechanism is the so-called chemical activation process. The association of O with CH_2OH produces the chemical activated (i.e., energy rich) OCH_2OH adduct because of the reaction exothermicity. Subsequently, the OCH_2OH radical may decompose or isomerize to form the final products. The second mechanism is the hydrogen abstraction processes by an O atom from either the OH group or the CH_2 group of the CH_2OH radical, forming either OH + CH_2O or OH + HCOH. The corresponding geometries of the intermediates and transition states involved in both mechanisms are shown in Figure 1. The potential energy surface is shown schematically in Figure 2. The calculated energies are summarized in Tables 1 and 2.

It has been demonstrated that the couple-cluster method shows good performance in the optimization of both minimum and transition state. As could be seen in Figure 1, the CCSD/cc-pVTZ optimized geometrical parameters are very close to those at the CCSD/cc-pVDZ level. Most of the changes in bond distances and angles are less than 0.02 Å and 1°, respectively. This indicates that the structures converge with the basis sets at the CCSD level. In addition, in Table 1, the heats of reaction obtained at the RCCSD(T)-cf level and the RCCSD(T)/CBS limit are both in good agreement with the available experimental data. The difference of the relative energies between RCCSD(T)-cf and RCCSD(T)/CBS is less than 2 kcal/mol. The accuracy

TABLE 1: Calculated Relative Energies (ΔE, in kcal/mol) and Zero-Point Energies (ZPE, in kcal/mol) of the Species Involved in the Addition/Elimination Mechanism of the $O(^3P) + CH_2OH$ Reaction

species	ZPE	ΔE [CCSD/VDZ]	ΔE [CCSD/VTZ]	ΔE_{cf} [RCCSD(T)/VQZ]	ΔE [RCCSD(T)/CBS]	exptl[a]
$O + CH_2OH$	23.83	0	0	0	0	
$OCH_2OH(^2A'')$	26.74	−78.8	−86.3	−91.1	−92.4	
$OCH_2OH(^2A)$	27.21	−81.6	−88.7	−93.3	−94.5	
TS1	22.92	−67.5	−73.4	−81.4	−82.2	
TS2	25.17	−54.8	−60.4	−60.9	−61.4	
TS3	24.30	−51.6	−57.3	−66.9	−67.2	
TS4	22.54	−5.1	−10.3	−21.6	−22.5	
TS5[b]	20.76			−2.9	−3.1	
TS6	24.63	−51.9	−60.5	−68.9	−70.2	
$HC(OH)_2$	27.73	−86.9	−95.4	−102.1	−103.8	
TS7	22.54	−62.8	−68.9	−77.5	−78.7	
TS8	24.17	−43.5	−50.8	−60.5	−61.3	
TS9	21.28	−14.6	−21.2	−32.3	−33.2	
$H + HCOOH$	21.66	−81.8	−85.5	−93.1	−93.7	−95.2
$CH_2O + OH$	22.25	−64.5	−68.0	−72.7	−73.3	−73.9
$HCO + H_2O$	21.82	−88.3	−94.3	−102.8	−104.0	−104
$H_2 + HCO_2$	18.86	−71.9	−74.0	−85.7	−84.3	
$H_2 + HOCO$	19.64	−86.7	−90.3	−100.1	−99.6	−101.8
$OH + HCOH$	21.86	−8.4	−11.4	−16.6	−17.1	

[a] The experimental enthalpies of formation are taken from ref 24. [b] The data are calculated at the MP2/cc-pVTZ optimized geometry.

TABLE 2: Calculated Energies at Various Levels of Theory for the Abstraction Paths[a]

level of theory	$O + CH_2OH$	**TSabs-1**	**TSabs-2**
CAS(5,5)/cc-pVDZ	−189.22800	−189.20789 (12.6)[b]	−189.20830 (12.4)
CAS(5,5)/cc-PVTZ	−189.28482	−189.26653 (11.5)	−189.26487 (12.5)
CASPT2/cc-pVDZ//CAS(5,5)/cc-pVDZ	−189.60584	−189.63867 (−20.6)	−189.59615 (6.1)
CASPT2/cc-pVTZ//CAS(5,5)/cc-pVDZ	−189.82735	−189.86508 (−23.7)	−189.81914 (5.2)
CASPT2/cc-pVTZ//CAS(5,5)/cc-pVTZ	−189.82765	−189.87663 (−30.7)	−189.81945 (5.1)
CISD/cc-pVDZ	−189.64578	−189.60176 (27.6)	
CISD/cc-pVTZ	−189.84807	−189.79767 (31.6)	
CCSD(T)/cc-pVTZ//CISD/cc-pVTZ	−189.86163	−189.86239 (−0.5)	
MRCISD/cc-pVTZ//CAS(5,5)/cc-pVTZ	−189.78861	−189.79326 (−2.9)	−189.77949 (5.7)
MRCISD/cc-pVTZ + Davidson//CAS(5,5)/cc-pVTZ	−189.84678	−189.85780 (−6.9)	−189.84582 (0.6)
MRCISD(19,13)/cc-pVTZ//CAS(5,5)/cc-pVTZ	−189.79576	−189.80175 (−3.8)	
MRCISD(19,13)/cc-pVTZ + Davidson//CAS(5,5)/cc-pVTZ	−189.84558	−189.85911 (−8.5)	
G3MP2//CAS(5,5)cc-pVTZ	−189.92469	−189.92707 (−1.5)	−189.90989 (9.3)

[a] A//B indicates the single-point energy calculation at level A using the geometry optimized at level B. [b] The values in parentheses stand for the barrier heights (in kilocalories per mole) with zero-point energy corrections.

of the barrier heights will be assessed below by kinetic analysis. The current potential energy surface is reliable within the "chemical accuracy" ($\sim \pm 2$ kcal/mol).

The two mechanisms will be discussed in detail as follows. Unless stated otherwise, the CCSD/cc-pVTZ structures and the RCCSD(T)/CBS energies will be used.

(1) Chemical Activation Mechanism. *(a) The OCH_2OH Radical.* The addition of $O(^3P)$ to the radical center of CH_2OH (i.e., C atom) proceeds on a barrierless, attractive surface. The newly formed CO bond in the OCH_2OH intermediate is around 1.35 Å. As could be seen from Figure 2, this addition step is exothermic by 94.5 kcal/mol. Therefore, the OCH_2OH radical could be highly activated.

As shown in Figure 1, the OCH_2OH radical has two conformations. One has C_s symmetry with a $^2A''$ electronic state. The other one has no symmetry. Both structures have almost identical geometrical parameters except for the HOCO dihedral angle. Energetically, the unsymmetrical OCH_2OH is about 2 kcal/mol more stable than the $^2A''$ structure. The two isomers undergo via an internal rotation of the OH group around the CO bond an interconversion. The profile of the potential energy for this internal rotation was calculated at the CCSD/cc-pVDZ level. The dihedral angle OCOH was scanned in an interval of 10°, and the remaining coordinates were optimized. The result is shown in Figure 3. Evidently, there are two saddle points along the internal rotation path with $\angle HOCO \approx 150$ and 0°, respectively. Meanwhile, the $^2A''$ structure is readily converted to the unsymmetrical structure because the barrier is very small.

Since a great amount of energy is deposited into the OCH_2OH adduct, lots of the subsequent reactions are able to occur.

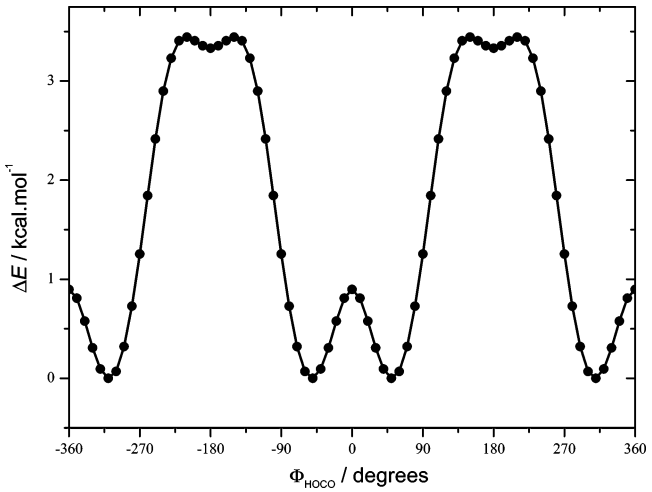

Figure 3. Energy profile for the internal rotation of OCH_2OH around the OCH_2−OH bond. The relative energy (ΔE, in kilocalories per mole) was calculated at the CCSD/cc-pVDZ level without zero-point energy correction.

Among them, simple bond fission, three- or four-center decomposition, and isomerization have been found.

(b) Simple Bond Fission Channels. There are two simple bond fission channels. The first one is to break the CH bond to form H and HCOOH (formic acid). The corresponding transition state is denoted as **TS1** in Figure 1. The breaking CH bond is stretched to about 1.6 Å, which is about 0.5 Å longer than the length of the CH bond in the equilibrium OCH_2OH radical. Meanwhile, the CO bond is shortened to 1.22 Å, which is very close to the length of the CO double bond in HCOOH. Clearly, **TS1** is a late transition state. The barrier height is 12.3 kcal/mol. It is noted that the CH bond fission possesses the lowest barrier in the present system. Moreover, it is interesting to note that the formation of H + HCOOH is almost thermoneutral.

The above decomposition path of the OCH_2OH radical was studied previously by Henon et al. at the B3LYP, MP2, and CCSD(T) levels with the cc-pVDZ basis set.[16] In comparison with the MP2/cc-pVDZ optimized geometrical parameters of **TS1**, the present **TS1** structure shows a more productlike character. For example, the breaking CH bond is 1.47 Å at the MP2/cc-pVDZ level, which is about 0.12 Å shorter than the present value (1.6 Å) at the CCSD/cc-pVTZ level. It implies that both the electron correlation and the basis set may affect the structure of the transition state. Coincidently, the present barrier height is in good agreement with the value 12.1 kcal/mol reported by Henon et al. at the CCSD(T)/cc-pVDZ level. The B3LYP and G2 calculations of Henon et al. gave barrier heights of 13.9 and 9.9 kcal/mol, respectively.

The second bond fission channel is to break the CO bond to form OH and CH_2O (formaldehyde). The corresponding transition state is denoted as **TS2** in Figure 1. The breaking CO bond is stretched to 1.88 Å, which is about 30% longer than the corresponding CO bond distance in the OCH_2OH radical. The other CO bond is shortened to 1.24 Å and tends to be a double bond. Evidently, **TS2** is a productlike transition state, in accordance with the fact that the $OCH_2OH \rightarrow CH_2O + OH$ reaction is highly endothermic by 21.2 kcal/mol. The barrier height for this decomposition is about 33.1 kcal/mol.

Henon et al. also studied the above CO bond rupture at the B3LYP/6-31G** level.[16] In contrast, they obtained a more productlike transition state with the breaking CO bond of 2.03 Å, which is about 0.15 Å longer than the present value. As a result, the calculated barrier height is 27 kcal/mol, which is 6 kcal/mol lower than our result. The large discrepancy just indicates that the low-level B3LYP/6-31G** method is not good or quantitative enough to deal with the bond-breaking reactions.

(c) Three- and Four-Center Decomposition of OCH_2OH. The first three-center decomposition channel is the production of HCO and H_2O via transition state **TS3** (see Figure 1). This is a very interesting process in view of the geometrical feature of **TS3**. The breaking CO bond is stretched to as long as 1.83 Å. In contrast, the other breaking CH bond is only slightly stretched to 1.13 Å, which is only 3% longer than its equilibrium value in OCH_2OH. Meanwhile, the forming OH bond is 1.73 Å, which is considerably longer than the equilibrium length in the product H_2O. Such a unique character of the transition state has been found for the three-center, one-step decomposition of the other substituted alkoxy radicals, for example, $CH_2ClO \rightarrow HCl + HCO$, $CH_2FO \rightarrow HF + HCO$, $CHCl_2O \rightarrow HCl + HCO$, $CHFClO \rightarrow HCl + FCO$, and so forth.[17−20] In addition, it is worth noting that **TS3** is very difficult to optimize. In comparison with **TS2**, it appears that **TS3** and **TS2** locate on the adjacent region of the potential energy surface because they have similar structure characters. For example, the breaking CO bonds have almost the same distances. The only difference of **TS3** from **TS2** is that one of the CH bonds is moving toward the OH group while it is stretched. The barrier height for **TS3** is about 27.3 kcal/mol. The current three-center decomposition channel is exothermic by about 9.5 kcal/mol.

All attempts to locate the transition state to connect the OCH_2-OH radical with the ground state H_2 + HOCO(X^2A') products have failed. It has been shown that the concept of the conventional "transition state" breaks down for the analogous three-center reaction, that is, $CH_3O \rightarrow H_2 + HCO$.[21] Such a decomposition path only possesses a barrier but without a transition state. To clarify this kind of three-center reaction, one needs the direct dynamics simulation. However, a second-order saddle point leading to H_2 and HOCO($^2A''$) was found, which is denoted as **TS4** in Figure 1. **TS4** has two imaginary frequencies. The normal mode of the first imaginary frequency corresponds to the symmetrical stretch of the two breaking CH bonds, whereas the other corresponds to the out-of-plane vibration of the OH bond.

The four-center decomposition of OCH_2OH forms H_2 + HCO_2 via transition state **TS5**. It is noted that **TS5** can only be optimized using the MP2 method. All the couple-cluster calculations have failed due to the problem of convergence in the optimization. As shown in Figure 2, both **TS4** and **TS5** are extremely high barriers. Thus, both the H_2 + HOCO and H_2 + HCO product channels are negligible. Neither H_2 nor HCO_2 nor HOCO nor CO_2 was observed experimentally.[2]

(d) Isomerization Channel. The OCH_2OH radical may rearrange into the $HC(OH)_2$ radical via the three-center H-shift transition state **TS6**, as shown in Figure 1. One of the hydrogen atoms migrates from C to O. The breaking CH bond and the forming OH bond are 1.27 and 1.21 Å, respectively. The other geometrical parameters almost do not change in the rearrangement. The barrier height is 24.3 kcal/mol, which is nearly twice the lowest barrier **TS1** but lower than **TS2** and **TS3**. The $HC(OH)_2$ radical has no symmetry. The two CO bond distances in $HC(OH)_2$ are slightly different. The radical center is located on the C atom. The energy of $HC(OH)_2$ is lower than that of OCH_2OH by about 9.3 kcal/mol.

The $HC(OH)_2$ radical could decompose subsequently. Three product channels have been studied. The first channel is to form H + HCOOH. The corresponding transition state is denoted as **TS7** in Figure 1. This is a simple HO bond rupture process.

The breaking OH bond is stretched to 1.38 Å. Simultaneously, the CO bond is shortened to 1.23 Å, which is close to the CO double bond in the HCOOH product. For consistency, the barrier height was calculated with respect to the OCH_2OH radical. A value of 15.8 kcal/mol was obtained for **TS7**. This is the lowest barrier among all of the decomposition channels of the HC(OH) radical. It is interesting to note that the decomposition of the OCH_2OH radical to form H + HCOOH also has the lowest barrier. The transition state **TS1** is about 3.5 kcal/mol lower than **TS7**.

There are two more bond cleavage channels leading to H + $C(OH)_2$ and OH + HCOH, respectively. Both channels are highly endothermic with respect to the HC(OH) radical. Tentative calculation shows that both channels proceed without any additional barriers. Therefore, these two bond cleavage channels are unimportant.

The second decomposition channel of $HC(OH)_2$ is the formation of HCO and H_2O. The corresponding transition state, **TS8**, is a four-center structure. Evidently, **TS8** is a productlike transition state. The forming OH bond is 1.16 Å, which is about 0.2 Å longer than the equilibrium OH distance in a water molecule. The barrier height is 33.2 kcal/mol. The third channel also involves a four-center transition state, denoted as **TS9** in Figure 1. The OH and CH bonds are breaking simultaneously with the formation of the HH bond. The products are the H_2 molecule and the $HOCO(^2A')$ radical. This process possesses a significant barrier, which is 61.3 kcal/mol.

In summary, three product channels could be determined in the chemical activation mechanism. In view of the barrier heights, the most favorable channel is the formation of H + HCOOH. Thus, it is suggested that the O + CH_2OH reaction might be responsible for the formation of formic acid in the oxidation of methanol. The other two minor channels are HCO + H_2O and CH_2O + OH, respectively. It should be noted that, although all channels involve barriers, as shown in Figure 2, all those barriers are below the initial reactants, O + CH_2OH. Moreover, all three product channels are highly exothermic. As a result, the highly vibrationally excited products, for instance, the hot HCOOH and CO molecules, are expected.

(2) The Direct Abstraction Mechanism. Besides the chemical activation mechanism, it was found that the one-step abstraction mechanism might play an important role in the O + CH_2OH reaction, even though it is a radical−radical reaction. As mentioned above, the multireference ab initio method is required to investigate the abstraction reaction. In the present calculation, the CASSCF(5,5) method was employed with both the cc-pVDZ and cc-pVTZ basis sets in the geometrical optimization.

There are two types of abstraction pathways. The first is the hydrogen abstraction by O from the CH_2 group. The corresponding transition state is shown in Figure 1 as **TSabs-1**. The breaking CH bond is stretched to about 1.28 Å, and the forming OH bond is around 1.22 Å. The CHO bond angle is about 117°, which is far away from linearity. Because the CASSCF calculation does not include the dynamic electron correlation, the other ab initio methods have been tried in order to locate **TSabs-1**. Unfortunately, most of them including MP2 and CCSD failed to get the optimized geometry except for the configuration interaction (CI) method. For comparison, the CISD/cc-pVDZ and CISD/cc-pVTZ optimized geometrical parameters are listed in Figure 1. It is evident that the CISD results show some differences from the CASSCF data. For example, the CISD method predicts the longer OH bond, the shorter CH bond, and the larger CHO bond angle. The production of OH and HCOH is exothermic by about 17 kcal/mol.

The second route is the direct hydrogen atom abstraction by O from the OH group, forming OH and CH_2O. The structure of the transition state is shown as **TSabs-2** in Figure 1. The breaking OH bond is only slightly stretched by about 0.05 Å. The forming OH bond is about 1.5 Å, which is more than 0.5 Å longer than the equilibrium OH bond distance. Moreover, the CO bond is 1.31 Å, which is only slightly shorter than the corresponding CO bond in the CH_2OH reactant. Evidently, **TSabs-2** shows reactant-like character; that is, it is an early barrier. The production of OH + CH_2O is highly exothermic by about 73 kcal/mol.

The barrier heights for both abstraction routes have been calculated by various high-level ab initio methods, including the multireference MP2 (CASPT2), multireference CI (MRCISD) with Davidson's correction. Some single-reference methods such as the CCSD(T) and G3MP2[22] methods were also employed in the calculation. The results are summarized in Table 2. For the O + CH_2OH reactants, the supermolecule approximation was used with the separation of the center of mass being 1000 Å. At the CASSCF/cc-pVTZ level, the barrier heights are predicted to be 11.5 and 12.5 kcal/mol for **TSabs-1** and **TSabs-2**, respectively. However, at higher levels, the calculated barrier heights decrease dramatically. For example, at the MRCISD/cc-pVTZ + Davidson level at the CASSCF/cc-pVTZ geometry, the energy of **TSabs-1** is calculated to be lower than that of the reactants by about 6 kcal/mol. It indicates that there is no barrier for such a hydrogen abstraction reaction. Meanwhile, the barrier for **TSabs-2** drops to only 0.6 kcal/mol at the same level. Additionally, it is worth noting that the zero-point energy correction for **TSabs-2** is more significant than that for **TSabs-1**. The CASPT2, CCSD(T), and G3MP2 calculations give similar conclusions, even though the CASPT2 data appear to be artifacts because of the "intrude state" problem from the small active space used in the calculation. In short, by analyzing the data in Table 2, it appears that the present two hydrogen abstractions by an O atom from the CH_2OH radical are almost barrierless. They might be able to compete with the chemical activation mechanism and thus play an important role in the O + CH_2OH reaction.

Only formic acid (HCOOH) and formaldehyde (CH_2O) have been observed by mass spectroscopy, although the other unidentified products cannot be excluded due to the detection sensitivity. On the basis of the potential energy surface, as shown in Figure 2, it is clear that the HCOOH molecule can only be produce via the chemical activation mechanism. The observed CH_2O experimentally should mainly originate from the direct abstraction routes. The CH_2O production channel in the chemical activation mechanism is less important. Moreover, since the mass spectroscopy cannot distinguish CH_2O and HCOH, the observed species at $m/e = 30$ might be a mixture of CH_2O and HCOH. It is desirable to use new experimental techniques to study the products in the O + CH_2OH reaction. For example, the detection of the OH radical by laser-induced fluorescence (LIF) is very helpful for determining the importance of the direct abstraction routes.

(3) Kinetics Analysis. Experimentally, the yields of HCOOH and CH_2O have not been determined because of the influence of the side reactions. Unfortunately, with the present ab initio data, we are not capable of predicting the relative yields, either. First, the statistical RRKM theory might not be rigorous in the treatment of the activated complexes OCH_2OH and $HC(OH)_2$.

In fact, the association is extremely exothermic so that the activated OCH_2OH radical might not have enough time to redistribute its available energy statistically. Second, the kinetic calculation for the abstraction reactions needs an accurate potential energy surface, which cannot be constructed readily. Note that the conventional dynamic calculation based on the minimum energy path (MEP) from the intrinsic reaction coordinate (IRC) is not appreciable because both abstractions are essentially barrierless even though an artificial MEP exists at the lower levels of theory. However, we are able to do the kinetic calculations on the following two specific processes.

First, the high-pressure limit rate constant for the association step of O with CH_2OH can be calculated as a function of temperature using the variational transition state theory because the association is governed only by the interaction between the O(^{3}P) atom and the C atom of CH_2OH.

Second, the falloff behavior of the OCH_2OH radical can be studied using the master equation analysis. Although this kind of calculation is less meaningful for the O + CH_2OH reaction, the thermalized OCH_2OH itself exists in the atmosphere and the kinetics of its decomposition is valuable to be known. Moreover, by calculating the kinetic data for the unimolecular reactions of OCH_2OH, we can estimate the uncertainty of the energies (especially the barrier heights) in this work. Therefore, the $OCH_2OH \rightarrow H + HCOOH$ reaction was analyzed because it is the most important decomposition channel, as shown in Figure 1, and the experimental data are available for comparison.

(a) Association Kinetics. As mentioned above, in the chemical activation mechanism, all barriers are far below the O + CH_2-OH reactants and the formation of the OCH_2OH radical is highly exothermic. Therefore, the lifetime of the activated OCH_2OH radical is very short. Once it is formed, it will fall apart very quickly. As a result, no pressure dependence for the association reaction is expected, as confirmed experimentally.

To calculate the temperature-dependent rate constant for the association, the energy profile for the addition of O(^{3}P) to the radical center (i.e., C atom) of the CH_2OH radical was obtained at the CASSCF(5,5)/cc-pVDZ level. The approaching OC distances vary from 3.0 to 5.0 Å, and the remaining geometrical parameters are optimized. To account for the dynamic electron correlation, the CASSCF(5,5)/cc-pVDZ energies were scaled by a factor of 1.34, which corresponds to the ratio of the dissociation energies (D_e) of OCH_2OH, calculated at the CAS-(5,5)/cc-pVDZ level (~73 kcal/mol) and the RCCSD(T)/CBS level (~98 kcal/mol), respectively, The results are shown in Figure 4. For convenience, the scaled energy profile was fitted by a Morse potential function, V_M(kcal/mol) = 98 $(1 - e^{-2.413(R_{OC}-1.25)})^2 - 98$, to describe the "minimum energy path" for the association approximately. A potential anisotropy form assuming a bonding potential which is cylindrically symmetric was also employed [e.g., $V = V_M \cos^n(\alpha-\alpha_e)$]. The exponent n of the angular dependence function is 2, and the equilibrium bond angle (α_e) for the CH_2OH fragment was set to 114.5°, that is, the equilibrium bond angle of OCO in OCH_2OH(^{2}A) at the CASSCF(5,5)/cc-pVDZ level of theory. The interactions between O(^{3}P) and H and O atoms of CH_2OH were calculated using additive pairwise atom−atom Lennard-Jones(12-6) potentials with the following parameters: $\sigma_O = 2.95$, $\sigma_H = 2.81$, $\epsilon_O = 42.8$, and $\epsilon_H = 5.98$ (σ values in angstroms and ϵ values in inverted centimeters). Then, the association rate constants were calculated using the flexible transition state theory at the E/J resolved level, as implemented in the Variflex code.[15] To evaluate the partition functions of transition states, the variable reaction coordinate (VRC) approach is used to treat the transitional modes. The reaction coordinates are defined as the separation between two pivot points located at O(^{3}P) and the C atom of CH_2OH, respectively. The range of reaction coordinates is between 3.0 and 5.0 Å in a step size of 0.05 Å. The transitional mode contribution to the transition state number of states for a given energy is evaluated via Monte Carlo integration using 10 000 configurations sampled in the random sampling. The convolution of the transitional and conserved modes over E and J has been carefully checked to ensure the convergence of the final thermal integrals. The required data including the vibrational frequencies and the Cartesian coordinates of CH_2-OH are taken from the CASSCF(5,5)/cc-pVDZ calculation directly. The rate constants were calculated in the temperature range 250−1000 K. It is noted that there are two nearly degenerate reactive surfaces for the O(^{3}P) + CH_2OH reaction. For simplicity, it is assumed that the O(^{3}P) + CH_2OH reaction has the same rates on both surfaces. Thus, the rate constants have been multiplied by a factor of 2 to account for such degeneracy. The results are shown in Figure 5.

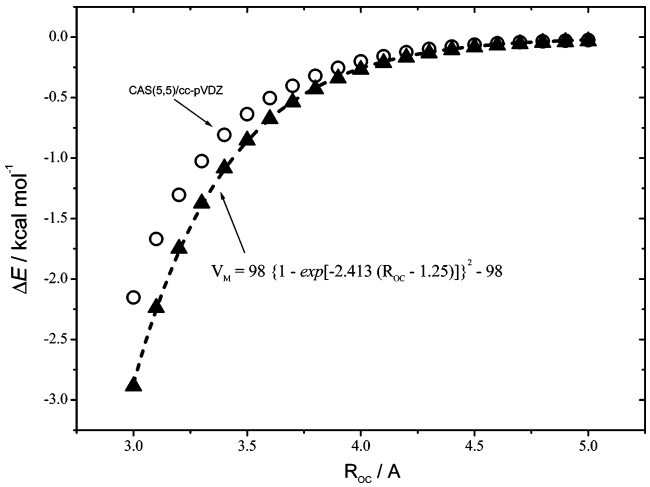

Figure 4. Minimum energy reaction path for the O + CH_2OH association. The relative energy (ΔE, in kilocalories per mole) was calculated at the CASSCF(5,5)/cc-pVDZ level (circles) with respect to O + CH_2OH. The OC distance (R_{OC}) was scanned with a step size of 0.1 Å. Triangles: scaled by a factor of 1.34. Dashed line: fitted by a Morse potential function.

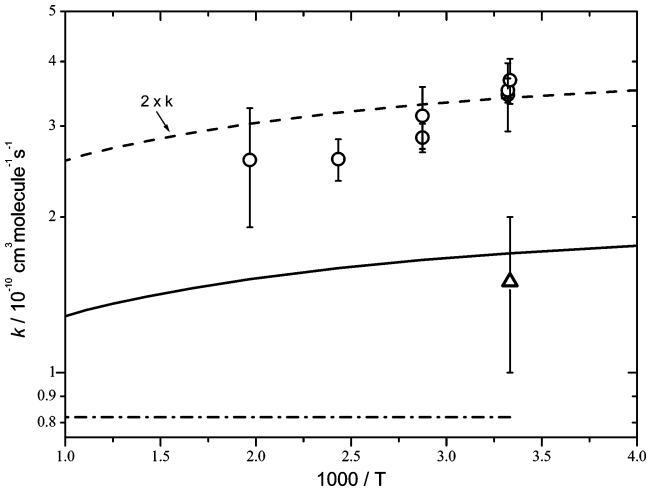

Figure 5. High-pressure limit rate constants for the association path of the O(^{3}P) + $CH_2OH \rightarrow OCH_2OH$ reaction. Solid line: this work. Dashed line: two times the calculated rate constants. Circles: ref 2. Triangle: ref 1. Dash−dotted line: ref 23.

The theoretical rate constants show a weak negative temperature dependence in the range 250−1000 K. This is a typical

behavior for the radical−radical association reactions. Experimentally, the overall rate constants for the O + CH_2OH reaction have been measured in the range 300−508 K.[2] The experimental data are included in Figure 5 for comparison. It is obvious that the theoretical values are smaller than the experimental data. The discrepancy is due to the fact that the abstraction reactions are not included in the calculation of the rate constants. At present, we can estimate the contribution of the abstraction channel to the overall reaction rates. As shown in Figure 5, good agreement between theory and experiment could be obtained if the theoretical rate constants are increased by a factor of 2. This indicates that the abstraction might play an important role in the O + CH_2OH reaction. However, the uncertainties in the calculated association rate constants make it impossible to obtain the absolute branching ratio of the abstraction reaction by the comparison in Figure 5.

The other experimental data shown in Figure 5 include the indirect measurement of the rate constant at room temperature by Grotheer et al.[1] A value of 1.5×10^{-10} cm^3 molecule^{-1} s^{-1} is about half of the direct measurement. In addition, Herron's recommendation[23] on the rate constant for the O + CH_2OH reaction is even smaller, only 8.2×10^{-11} cm^3 molecule^{-1} s^{-1} in the range 300−3000 K.

(b) Falloff Kinetics of the $OCH_2OH \rightarrow H + HCOOH$ Reaction and the Uncertainty of the PES. There is not a conventional method for estimating the uncertainty of the ab initio calculated energies in this work. As could be seen in Table 1, the calculated heats of reaction (ΔH) at 0 K deviate from the experimental values by 0.2−1.5 kcal/mol.[24] However, it is much harder to assess the uncertainty of the barrier height. Fortunately, the $OCH_2OH \rightarrow H + HCOOH$ reaction has been studied experimentally by Veyret et al.[25] On the basis of the model study of a complex mechanism, the rate constant was proposed to be around 1200 s^{-1} at 298 K and a 10−30 Torr total pressure of formaldehyde.

It is noted that Henon et al. performed a RRKM-type analysis for the $OCH_2OH \rightarrow H + HCOOH$ reaction.[16] However, there is a serious drawback in their calculation; that is, the tunneling effect was not considered. The existence of a significant tunneling effect in this CH bond rapture process could be seen from the large imaginary frequency of 1342 cm^{-1}. Usually, the tunneling effect cannot be neglected for the reactions involving a H atom. Without the tunneling effect, the barrier height for the $OCH_2OH \rightarrow H + HCOOH$ reaction was adjusted to 9.6 kcal/mol to fit the experimental values by Henon et al. This conclusion could be misleading.

In this work, the falloff curve has been calculated by solving the master equation (ME) at the E/J resolved level.[26] As expected, the variational effect is negligible. The tunneling effect was taken into account using an Eckart potential.[27] The rigid-rotor harmonic oscillator (RRHO) approximation was used for the transition state (**TS1**). The exponential down model was used for the energy transfer process. Because the energy transfer parameter ($\langle \Delta E_{down} \rangle$) for the OCH_2OH-CH_2O collision is not available, it is set to be an adjustable parameter or is estimated by the biased random walk (BRW) model.[28]

The tunneling effect was investigated first. The $\langle \Delta E_{down} \rangle$ value is 140 cm^{-1} from the BRW model. As could be seen in Figure 6, the tunneling effect plays an important role in the reaction. Without tunneling, the calculated rate constants are considerably lower than the experimental data. With tunneling, the rate constants become significantly larger. Moreover, the tunneling effect makes the rate constants decrease much more slowly.

However, it is evident that the calculated rate constants are larger than the experimental data in the range 10−30 Torr by more than 1 order of magnitude. In the present calculation, three parameters might be adjusted to fit the experimental data, including the barrier height, the $\langle \Delta E_{down} \rangle$ value, and the imaginary frequency (ν_{img}) for the transition state. The results are shown in Figure 6 for comparison.

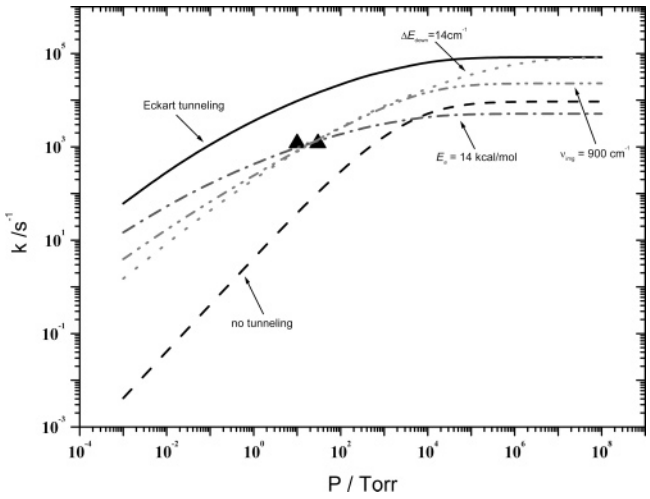

Figure 6. Falloff curve at 298 K for the $OCH_2OH \rightarrow H + HCOOH$ reaction. Triangles: the experimental data in ref 25. Solid line: with Eckart tunneling correction, the barrier height ΔE = 12.3 kcal/mol, the energy transfer parameter $\langle \Delta E_{down} \rangle$ = 140 cm^{-1}, and the imaginary frequency ν_{img} = 1342 cm^{-1}. Dashed line: without tunneling correction, ΔE = 12.3 kcal/mol, and $\langle \Delta E_{down} \rangle$ = 140 cm^{-1}. Dotted line: with Eckart tunneling correction, ΔE = 12.3 kcal/mol, $\langle \Delta E_{down} \rangle$ = 14 cm^{-1}, and ν_{img} = 1342 cm^{-1}. Dash−dotted line: with Eckart tunneling correction, ΔE = 14 kcal/mol, $\langle \Delta E_{down} \rangle$ = 140 cm^{-1}, and ν_{img} =1342 cm^{-1}. Dash−dot−dotted line: with Eckart tunneling correction, ΔE = 12.3 kcal/mol, $\langle \Delta E_{down} \rangle$ = 140 cm^{-1}, and ν_{img} = 900 cm^{-1} (see text for details).

If a barrier height of 12.3 kcal/mol and an imaginary frequency of 1342 cm^{-1} from the ab initio calculations are chosen, a very small value of $\langle \Delta E_{down} \rangle$ = 14 cm^{-1} has to be used to fit the experimental data. This is an unreasonable value for the OCH_2OH-CH_2O collisional system because usually formaldehyde is thought to be an effective quencher. Therefore, the $\langle \Delta E_{down} \rangle$ = 140 cm^{-1} value has been fixed to check the uncertainty in the barrier height and the imaginary frequency, which are expected to be the key origin of the large discrepancy between the theoretical rate constants and the experimental data. If the imaginary frequency is fixed to 1342 cm^{-1}, as indicated in Figure 6, the barrier height has to increase by 1.7 kcal/mol, and the agreement between theory and experiment is excellent. On the other hand, if the barrier height is fixed to 12.3 kcal/mol, the imaginary frequency should be lowered to about 900 cm^{-1} to obtain the agreement between theory and experiment. We do not know which adjustment is better because both of them appear to be reasonable.

As a result, it is estimated that the potential energy surface in this work has an uncertainty of about 2 kcal/mol, which reaches the so-called chemical accuracy. In addition, it appears that the best-fit value 9.6 kcal/mol obtained by Henon et al. for the barrier height of the $OCH_2OH \rightarrow H + HCOOH$ reaction might be misleading. Of course, the question still remains on the energy transfer parameter ($\langle \Delta E_{down} \rangle$) and the imaginary frequency, in other words, the tunneling effect.

IV. Conclusions

Ab initio computations have been performed for the O(^{3}P) + CH_2OH reaction. The title reaction proceeds via two mechanisms. The chemical activation mechanism involves the

association of an O atom with CH_2OH to form the OCH_2OH intermediate. Subsequent decomposition of OCH_2OH produces H + HCOOH dominantly. The other minor product channels include HCO + H_2O and OH + CH_2O. The direct hydrogen abstraction produces either OH + CH_2O or OH + HCOH. Both abstractions are essentially barrierless. The rate constants for the association of O + CH_2OH show typical negative temperature dependence in the range 250−1000 K. It is estimated that both the association and abstraction mechanisms play equally important roles in the O + CH_2OH reaction. Experimental detection of the OH radical is strongly desired.

By the simulation of the falloff behavior of the $OCH_2OH \rightarrow$ H + HCOOH reaction at 298 K, it is estimated that the present potential energy surface has an uncertainty of 2 kcal/mol. The tunneling effect plays an important role in this reaction.

Acknowledgment. This work was supported by the Foundation for the Author of National Excellent Doctoral Dissertation of China (no. 200224).

References and Notes

(1) Grotheer, H. H.; Rickert, G.; Walter, D.; Just, Th. *J. Phys. Chem.* **1988**, *92*, 4028.

(2) Seetula, J. A.; Kalinovski, I. J.; Slagle, I. R.; Gutman, D. *Chem. Phys. Lett.* **1994**, *224*, 533.

(3) Scuseria, G. E.; Schaefer, H. F., III. *J. Chem. Phys.* **1989**, *90*, 3700.

(4) Dunning, T. H., Jr. *J. Chem. Phys.* **1989**, *90*, 1007.

(5) Gonzalez, C.; Schlegel, H. B. *J. Phys. Chem.* **1990**, *94*, 5523.

(6) Knowles, P. J.; Hampel, C.; Werner, H.-J. *J. Chem. Phys.* **1993**, *99*, 5219.

(7) Goodson, D. Z. *J. Chem. Phys.* **2002**, *116*, 6948.

(8) Feller, D. *J. Chem. Phys.* **1992**, *96*, 6104.

(9) Helgaker, T.; Klopper, W.; Koch, H.; Noga, J. *J. Chem. Phys.* **1997**, *106*, 9639.

(10) Werner, H.-J.; Knowles, P. J. *J. Chem. Phys.* **1985**, *82*, 5053.

(11) Werner, H.-J. *Mol. Phys.* 1996, *89*, 645.

(12) Werner, H.-J.; Knowles, P. J. *J. Chem. Phys.* 1988, *89*, 5803.

(13) Frisch, M. J.; Trucks, G. W.; Schlegel, H. B.; Scuseria, G. E.; Robb, M. A.; Cheeseman, J. R.; Montgomery, J. A., Jr.; Vreven, T.; Kudin, K. N.; Burant, J. C.; Millam, J. M.; Iyengar, S. S.; Tomasi, J.; Barone, V.; Mennucci, B.; Cossi, M.; Scalmani, G.; Rega, N.; Petersson, G. A.; Nakatsuji, H.; Hada, M.; Ehara, M.; Toyota, K.; Fukuda, R.; Hasegawa, J.; Ishida, M.; Nakajima, T.; Honda, Y.; Kitao, O.; Nakai, H.; Klene, M.; Li, X.; Knox, J. E.; Hratchian, H. P.; Cross, J. B.; Adamo, C.; Jaramillo, J.; Gomperts, R.; Stratmann, R. E.; Yazyev, O.; Austin, A. J.; Cammi, R.; Pomelli, C.; Ochterski, J. W.; Ayala, P. Y.; Morokuma, K.; Voth, G. A.; Salvador, P.; Dannenberg, J. J.; Zakrzewski, V. G.; Dapprich, S.; Daniels, A. D.; Strain, M. C.; Farkas, O.; Malick, D. K.; Rabuck, A. D.; Raghavachari, K.; Foresman, J. B.; Ortiz, J. V.; Cui, Q.; Baboul, A. G.; Clifford, S.; Cioslowski, J.; Stefanov, B. B.; Liu, G.; Liashenko, A.; Piskorz, P.; Komaromi, I.; Martin, R. L.; Fox, D. J.; Keith, T.; Al-Laham, M. A.; Peng, C. Y.; Nanayakkara, A.; Challacombe, M.; Gill, P. M. W.; Johnson, B.; Chen, W.; Wong, M. W.; Gonzalez, C.; Pople, J. A. *Gaussian 03*, revision B.05; Gaussian, Inc.: Pittsburgh, PA, 2003.

(14) Molpro is a package of ab initio programs written by H.-J. Werner and P. J. Knowles, with contributions from R. D. Amos, A. Bernhardsson, A. Berning, P. Celani, D. L. Cooper, M. J. O. Deegan, A. J. Dobbyn, F. Eckert, C. Hampel, G. Hetzer, T. Korona, R. Lindh, A. W. Lloyd, S. J. McNicholas, F. R. Manby, W. Meyer, M. E. Mura, A. Nicklass, P. Palmieri, R. Pitzer, G. Rauhut, M. Schütz, H. Stoll, A. J. Stone, R. Tarroni, and T. Thorsteinsson.

(15) Klippenstein, S. J.; Wagner, A. F.; Dunbar, R. C.; Wardlaw, D. M.; Robertson, S. H. *Variflex*, version 1.00; 1999.

(16) Henon, E.; Bohr, F.; Gomez, N. S.; Caralp, F. *Phys. Chem. Chem. Phys.* **2003**, *5*, 5431.

(17) Wang, B.; Hou, H.; Gu, Y. *J. Phys. Chem. A* **1999**, *103*, 2060.

(18) Wang, B.; Hou, H.; Gu, Y. *Chem. Phys. Lett.* **1999**, *304*, 278.

(19) Hou, H.; Wang, B.; Gu, Y. *J. Phys. Chem. A* **1999**, *103*, 8075.

(20) Hou, H.; Wang, B.; Gu, Y. *J. Phys. Chem. A* **2000**, *104*, 1570.

(21) Marcy, T. P.; Diaz, R. R.; Heard, D.; Leone, S. R.; Harding, L. B.; Klippenstein, S. J. *J. Phys. Chem. A* **2001**, *105*, 8361.

(22) Curtiss, L. A.; Redfern, P. C.; Raghavachari, K.; Rassolov, V.; Pople, J. A. *J. Chem. Phys.* **1999**, *110*, 4703.

(23) Herron, J. T. *J. Phys. Chem. Ref. Data* **1988**, *17*, 967.

(24) Sander, S. P. *Chemical Kinetics and Photochemical Data for Use in Atmospheric Studies*, JPL Publication 02-25, Evaluation Number 14, **2003**, Appendix A-1 and reference therein.

(25) Veyret, B.; Roussel, P.; Lesclaux, R. *Int. J. Chem. Kinet.* **1984**, *16*, 1599.

(26) Gilbert, R. G.; Smith, S. C. *Theory of Unimolecular Reactions*; Blackwell: Oxford, 1990.

(27) Eckart, C. *Phys. Rev.* **1930**, *35*, 1303.

(28) Lim, K. F.; Gilbert, R. G. *J. Chem. Phys.* **1990**, *92*, 1819.